

Dynamical Jahn–Teller effect and antiferromagnetism in Cs_3C_{60}

Naoya Iwahara and Liviu F. Chibotaru

Division of Quantum and Physical Chemistry, Katholieke Universiteit Leuven, Celestijnenlaan 200F, B-3001 Leuven, Belgium

(Dated: June 25, 2021)

The dynamical Jahn–Teller effect on fullerene sites in insulating Cs_3C_{60} is investigated fully ab initio. The vibronic excitations of rotational type are at $\geq 65 \text{ cm}^{-1}$ while the net kinetic contribution to the Jahn–Teller stabilization energy constitutes ca 90 meV. This means that no localization of distortions by intermolecular interactions is possible in these fullerides, therefore, free rotations of deformations take place independently on each C_{60} . The latter destroy the orbital ordering and establish a conventional exchange interaction between $S = 1/2$ on fullerene sites. The corresponding exchange model is derived and predicts the Néel temperature for A15 Cs_3C_{60} close to experiment.

The alkali-doped fullerides A_3C_{60} attracted much attention in the past as prominent examples of purely organic high- T_c superconductors [1]. Recently a critical temperature of 38 K has been observed in the superconducting Cs_3C_{60} [2], reviving the interest for these fullerides due to their closeness to the Mott-Hubbard metal-insulator transition [3–7]. It was found that applying an external pressure (P) these materials can be brought from insulator to superconductor [2–4]. Such transformation was explained by the increase of the width w of the partly occupied threefold degenerate t_{1u} band under pressure, and the concomitant reduction of the ratio U/w (U is the intrafullerene electron repulsion parameter), which causes a Mott-Hubbard transition above some critical pressure. A thorough investigation of T_c in a wide range of applied pressures revealed its nonmonotonic dependence on pressure (or interfullerene distance) in the metallic phase [2]. The maximum of $T_c(P)$ testifies about non-BCS behaviour of Cs_3C_{60} close to Mott-Hubbard transition. The nonmonotonic behaviour of superconductivity has been qualitatively reproduced by dynamical mean-field calculations [8–10], which explained the decline of superconductivity close to Mott-Hubbard transition by the suppression of metallic (and superconducting) fraction of electronic density induced by strong electron correlation [9]. Furthermore, the NMR studies of these compounds [5–7] have evidenced that the maximum of $T_c(P)$ corresponds to the onset of the effects of strong electron correlation on superconductivity. Indeed, it was found that the nuclear spin lattice relaxation time T_1 for Cs_3C_{60} starts to deviate from a BCS-like dependence when the pressure is decreased from the value corresponding to the maximum of $T_c(P)$ towards the Mott-Hubbard transition [6]. At the same time, in the domain of higher pressure the dependence of T_1 vs interfullerene distance merges with the smooth curve found on the other A_3C_{60} compounds [11].

The similarity of the $T_c(P)$ dependence for Cs_3C_{60} with the dome structure of T_c on the T - n phase diagram for cuprates has tempted some authors to suppose a close mechanism of superconductivity, based on strong electron correlation, in both these materials. In the case of cuprates and iron pnictides there is a strong evidence

that superconducting pairing arises from magnetic fluctuations. However, in the case of fullerides such pairing mechanism is expected to be much less efficient because the exchange interaction in the latter amounts to few meV, i.e., is two orders of magnitude smaller than in cuprates. This points to the electron-phonon coupling as the main contribution to the pairing interaction in Cs_3C_{60} , as was already found for less correlated fullerides K_3C_{60} and Rb_3C_{60} [1]. The electron-phonon coupling in the LUMO band of fullerides comes mainly from the local vibrations of total-symmetric a_g and Jahn–Teller (JT) h_g type. The latter give 4-5 times larger contribution to the stabilization of an electron on fullerene site [12, 13], the same for the relative contribution to the superconducting pairing [1]. More importantly, it was found that the contribution of JT phonons to the superconducting pairing is suppressed by strong electron correlations at much lesser extent than the contribution from the total symmetric vibrations [9], making them a prime source of superconducting pairing in Cs_3C_{60} .

The actual role of Jahn–Teller effect (JTE) in fullerides gave rise to controversial opinions. It seems to be firmly established nowadays that cubic A_nC_{60} , $\text{A}=\text{K}, \text{Rb}, \text{Cs}$, $n=1-6$, show no static JT distortions in experiments probing their structure. Among the recent confirmations, the structural data from the synchrotron x-ray diffraction at 10 K shows no JT distortions of C_{60}^{3-} ions in Cs_3C_{60} fullerides [2, 3]. The absence of detectable JT distortions in the x-ray data of metallic fullerides was interpreted by many authors as their suppression by band effects. At the same time the non-observability of these distortions in insulating A_4C_{60} is considered to be due to their disordering and partial dynamic delocalization between different minima. In expanded cubic fullerides, deeply immersed in a Mott-Hubbard insulating state [14], a dynamical JTE of rotational type on fullerene sites was inferred [15]. Finally in insulating Cs_3C_{60} another type of dynamical JTE, corresponding to fast jumps between different local minima of potential energy surface, was claimed to be the reason for the observed features of the infrared spectra [16]. Note that in all these cases the details of JTE have not been known a priori but rather inferred from available experiment [12]. In this Letter

we present the first fully ab initio treatment of dynamical JTE on C_{60}^{3-} sites in insulating Cs_3C_{60} and show its crucial role for the observed magnetism in this fulleride.

In insulating Cs_3C_{60} the electrons from the t_{1u} band become localized at fullerene sites. The t_{1u}^3 shell of each trianion C_{60}^{3-} splits into three electronic terms, $^4S \oplus ^2P \oplus ^2D$, at an extent comparable to JT stabilization energy (vide infra). Formulated as mixing of the terms, the JT couplings appears only between the 2P and the 2D terms [17]. Using the complex wave functions of the terms $\{|^2P, M_P\rangle, |^2D, M_D\rangle; M_P = -1, 0, 1, M_D = -2, -1, 0, 1, 2\}$, the Hamiltonian matrix is given by

$$\hat{H} = \hat{H}_0 + \hat{H}_{JT} + \hat{H}_{ee}, \quad (1)$$

$$\hat{H}_0 = \sum_{\mu=1}^8 \sum_{m_v=-2}^2 \hbar\omega_{\mu} \hat{b}_{\mu,m_v}^{\dagger} \hat{b}_{\mu,m_v} \hat{I}, \quad (2)$$

$$\hat{H}_{JT} = \sum_{\mu=1}^8 \frac{\sqrt{3}}{2} \hbar\omega_{\mu} g_{\mu} \begin{pmatrix} \hat{O}_P & \hat{M}_{\mu} \\ \hat{M}_{\mu}^{\dagger} & \hat{O}_D \end{pmatrix}, \quad (3)$$

$$\hat{H}_{ee} = 2J_H \hat{I}_P. \quad (4)$$

Here, m_v denotes the complex basis for h_g vibrations [18], μ indexes the μ th h_g vibrational mode, ω_{μ} is the corresponding frequency, $\hat{b}_{\mu,m_v}^{\dagger}$ (\hat{b}_{μ,m_v}) is the creation (annihilation) operator of the vibration $\mu h_g m_v$, \hat{I}_{Γ} is the projection operator onto the term $\Gamma = P, D$ and $\hat{I} = \hat{I}_P + \hat{I}_D$, g_{μ} is the dimensionless orbital vibronic coupling constant, \hat{O}_P and \hat{O}_D are the 3×3 and the 5×5 zero matrices, \hat{M}_{μ} is defined by ($q_{m_v} \equiv q_{\mu m_v}$)

$$\hat{M}_{\mu} = \begin{pmatrix} \sqrt{2}q_{-1} & \sqrt{3}q_0 & \sqrt{3}q_1 & \sqrt{2}q_2 & 0 \\ -2q_{-2} & -q_{-1} & 0 & q_1 & 2q_2 \\ 0 & -\sqrt{2}q_{-2} & -\sqrt{3}q_{-1} & -\sqrt{3}q_0 & -\sqrt{2}q_1 \end{pmatrix} \quad (5)$$

with $q_{\mu,m_v} = [\hat{b}_{\mu,m_v}^{\dagger} + (-1)^{m_v} \hat{b}_{\mu,-m_v}]/\sqrt{2}$, and J_H is the Hund's rule coupling constant. In Eq. (1) the zero of energy corresponds to the energy of 2D term plus the zero-point vibrational energy.

The JT Hamiltonian (1) commutes with the vibronic angular momentum \hat{J}^2 and its projection \hat{J}_z [19], and with the 'parity' operator

$$\hat{P} = (\hat{I}_P - \hat{I}_D) \exp \left(i\pi \sum_{\mu=1}^8 \sum_{m_v=-2}^2 \hat{b}_{\mu,m_v}^{\dagger} \hat{b}_{\mu,m_v} \right), \quad (6)$$

which commute also between themselves. Then each vibronic state will be characterized the quantum numbers $J(=0, 1, 2, \dots)$, $M_z(=-J, -J+1, \dots, J)$ and $P(=\pm 1)$.

As g_{μ} in Eq. (3), we use the values calculated by density-functional theory (DFT) with hybrid B3LYP functional and those derived from the photoelectron spectrum (PES) of C_{60}^{-} (set (2) and (3) in Table S1 of Supplemental Material, respectively[26]) [13, 20]. Given the good comparison of calculated and measured g_{μ} 's for C_{60}^{-} (g_{μ} 's derived from several methods are compared in Table

TABLE I. Contributions to the ground state vibronic energy of C_{60}^{3-} (meV).

Set	Total	$\langle \hat{H}_{ee} \rangle$	JT stabilization	Static	Dynamic
(2)	-196.2	41.0	-237.2	-150.6	-86.6
(3)	-223.3	40.9	-264.2	-173.1	-91.1

V of Ref. 13), we applied the same approach to calculate orbital vibronic coupling constants on fullerene sites in Cs_3C_{60} [21]. To this end a fragment including one C_{60}^{3-} with nearest-neighbour Cs^{+} ions was considered in the Madelung field of the rest of the crystal. The results (set (1) in Table S1) prove to be remarkably close to the case of one isolated C_{60}^{-} (set (2) in Table S1). This means that the interaction with the lattice and the fullerene charging are insignificant for orbital vibronic constants. We applied the same DFT approach to evaluate the Hund's coupling constant for C_{60}^{3-} and obtained $J_H = 44$ meV which is close to the suggested value of about 50 meV [22]. Then, with experimental frequencies for the eight h_g modes [1], all terms of the Hamiltonian (1) are completely defined.

The JT Hamiltonian (1) was diagonalized numerically using the Lanczos method as in the case of C_{60}^{-} [12, 13]. However now the problem is more demanding because of a stronger JTE in C_{60}^{3-} and the need to mix all eight electronic wave functions of the terms 2P and 2D . The vibrational wave functions for each of them included linear combinations of products of uncoupled oscillators after 40 $\{\mu h_g m_v\}$ vibrations with total excitation not exceeding seven vibrational quanta.

The ground vibronic state corresponds to $J = 1$ and $P = 1$, i.e., is threefold degenerate after vibronic momentum. Table I shows that the total stabilization energy with respect to the 2D term (the ground doublet state in the absence of vibronic coupling) is ca 210 meV. This cannot be attributed solely to JT stabilization because JTE in this system implies mixing of 2D and 2P terms leading to the rise of electronic energy, Eq. (4), by ca 40 meV. Extracting this contribution from the total energy we obtain the JT stabilization energy of ca 250 meV. This consists of a stabilization energy due to equilibrium static JT distortions (when the kinetic energy of nuclei is neglected [19]) and due to dynamic delocalization of JT distortions in the three-dimensional trough of the ground state potential energy surface. The former contribution is three times the static JT stabilization energy for a singly charged fullerene [18] (E_{JT} in Table S1) and is ca 160 meV. Extracting this value from the total JT stabilization energy we obtain that ca 90 meV corresponds to the dynamic contribution, which is *more than half* of the static JT stabilization energy.

The low-lying vibronic states are characterized by consecutive increase of J (Table II). This quantum number

TABLE II. Energies of low-lying vibronic levels in C_{60}^{3-} (cm^{-1}) calculated for two sets of vibronic parameters.

(J, P)	Set (2)		Set (3)	
	exact	effective	exact	effective
(1, +1)	0	0	0	0
(2, -1)	65.7	65.8	63.6	63.9
(3, -1)	254.1	453.3	251.1	427.8
(4, +1)	283.0	393.9	273.8	369.1

corresponds to three-dimensional rotations of JT deformations in the trough of the lowest potential energy surface and its increase with the energy of low-lying levels is generally expected [19]. However the spacing between these levels differs drastically from the predictions of simplified vibronic models of C_{60}^{3-} [17, 18]. To get more insight into this problem we derive an effective one-mode $t^3 \times h$ JT Hamiltonian (retaining the bielectronic term, Eq. (4)) that reproduces the static JT stabilization (Table I) and the energy of the first excited vibronic level. For set 2 (3) we obtain the effective vibronic coupling constant $g_{\text{eff}} = 1.07$ (1.15) and the effective frequency for h_g vibrations $\omega_{\text{eff}} = 707$ (704) cm^{-1} . From the obtained g_{eff} we conclude that the JT effect in C_{60}^{3-} is of intermediate coupling strength. The dynamic contribution to JT stabilization differs by only 11 meV from the exact result. In the strong coupling limit this contribution is $(3/2)\hbar\omega_{\text{eff}}$ [17, 18], which is ca 50% higher. The excited states obtained with the effective one-mode JT Hamiltonian do not simulate well the low-lying vibronic spectrum, even give wrong order of levels (Table II). This contradicts the general belief that low-lying states of a multimode vibronic problem can be described satisfactorily by an effective one-mode Hamiltonian [17, 23].

The ground vibrational level of non-JT term 4S has the energy $E_0^{(3/2)} = -3J_H = -132$ meV, i.e., lies higher than the ground vibronic state of the spin doublet ($E_0^{(1/2)}$) by 64.2 and 91.3 meV for sets (2) and (3) in Table I, respectively. While the last value is close to the estimate for the spin gap in this material (0.1 eV) [5] we note that the activation energy for the spin quartet state should also include the difference of the entropy of vibrational levels for spin quartet ($\ln Z_{\text{vib}}^{(3/2)}$) and vibronic levels for spin doublet states ($\ln Z_{\text{vib}}^{(1/2)}$):

$$\Delta E^{(3/2)} = E_0^{(3/2)} - E_0^{(1/2)} - kT(\ln Z_{\text{vib}}^{(3/2)} - \ln Z_{\text{vib}}^{(1/2)}). \quad (7)$$

Dynamical JTE in the spin doublet state leads to a denser spectrum of vibronic levels as compared to vibrational spectrum of the spin quartet resulting in $Z_{\text{vib}}^{(1/2)} > Z_{\text{vib}}^{(3/2)}$ for any temperature. Then the entropic term in (7) will increase the activation energy for $T > 0$, which thus can rise significantly with temperature. This can explain why no contribution of $S = 3/2$ was seen for NMR relaxation

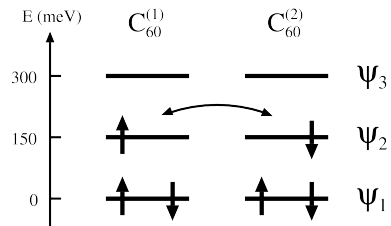


FIG. 1. Basic mechanism of a superexchange interaction between fullerene sites in insulating Cs_3C_{60} .

times in Cs_3C_{60} at room temperature [6].

The average value of $E_0^{(3/2)} - E_0^{(1/2)}$ (ca 80 meV) is comparable to the dynamic contribution to JT stabilization energy (last column in Table I). This means that if the JT deformations become localized by low-symmetric surrounding of C_{60}^{3-} or random strains, the vibronic levels will approach the vibrational spectrum, so that the dynamic contribution to JT stabilization will be quenched. As a result the spin gap $E_0^{(3/2)} - E_0^{(1/2)}$ will be strongly reduced, the same for the entropic term in Eq. (7) and the entire activation energy $\Delta E^{(3/2)}$. One should note, however, that the low-symmetric environment can itself lead to the splitting of the t_{1u} shell in undistorted fullerenes by several tens of meV [24] giving an independent contribution to the spin gap, that can thus survive in low-symmetry fullerenes.

In cubic environment the vibrational h_g modes of C_{60} split into t_g and e_g cubic modes leading to the warping of the adiabatic potential energy surface (APES). The energy difference between the resulting maxima and minima of the lowest APES can be expressed via the frequencies of the corresponding modes (ω_{t_g} and ω_{e_g}) as $2[(\omega_{e_g}^2 - \omega_{t_g}^2)/(\omega_{e_g}^2 + \omega_{t_g}^2)]E_{\text{JT}}$ [17]. Table S2 in Supplemental Material [26] gives the frequencies of t_g and e_g modes obtained from fragment DFT calculations of Cs_3C_{60} [21]. One can see that the splitting of h_g vibrations in this fulleride does not exceed few wavenumbers. Passing from frequencies in Table S2 to single effective t_g and e_g modes [17, 23], we estimate with the above formula the warping amplitude as 3.1 cm^{-1} , which proves to be too small to hinder the free rotations of JT deformations on C_{60}^{3-} (cf. the spacing of low-lying vibronic levels in Table II). On the other hand the second order JT effect in C_{60}^{3-} [23, 27–29] is expected to result in similar amplitude of warping of the lowest APES, as quantum chemistry calculations show [30, 31], and will not hinder the rotations of JT deformations either [32]. Finally, the magnetic interaction between fullerenes (of the order of Néel temperature, $T_N = 46 \text{ K}$ [2–7]) and the intermolecular phonons (with frequencies amounting to several tens of wavenumbers [1]) are comparable in energy with the lowest vibronic excitation (65 cm^{-1}) but are still much smaller than the dynamical contribution to JT stabilization.

TABLE III. Calculated exchange parameters (meV) and Néel temperatures and Weiss temperatures (K) for two sets of transfer integrals (meV), from the present work and from Nomura *et al.* [25].

	t_{xx}^{AB}	t_{yx}^{AB}	t_{zx}^{AB}	t_{xx}^{AA}	t_{yy}^{AA}	t_{zz}^{AA}	w	$J_{\text{ex}}^{\text{AB}}$	$J_{\text{ex}}^{\text{AA}}$	T_{N}	Θ
Present	-20.1	32.5	5.6	4.8	-17.6	-6.7	512	2.12	0.17	46	-52
Nomura	-20.6	32.9	5.3	7.3	-7.9	-18.0	535	2.18	0.20	48	-54

tion energy. We conclude, therefore, that each fullerene in Cs_3C_{60} is characterized by *unquenched rotations of JT deformations* in the trough of the lowest APES.

Accordingly, the exchange interaction between fullerene sites corresponds to averaging after nuclear coordinates over all points in the three-dimensional trough of each C_{60}^{3-} . The way this averaging is done and the resulting exchange mechanism depends on the structure of vibronic state. Overlap integrals of the ground vibronic states with spin doublet configurations $\psi_1^{n_1}\psi_2^{n_2}\psi_3^{n_3}$, $n_1 + n_2 + n_3 = 3$, of three adiabatic orbitals ψ_i (the ones which diagonalize the static JT problem for a given JT distortion) show that the ground configuration $\psi_1^2\psi_2^1$ (see Fig. 1) enters with the weight 0.86 and 0.87 for set (2) and (3), respectively. Such a high weight of a single adiabatic configuration is rather surprising given that C_{60}^{3-} is far from the strong coupling limit as was mentioned above. The main contribution to the exchange interaction between such adiabatic configurations of two fullerene ions comes from superexchange interaction between half filled adiabatic orbitals ψ_2 (Fig. 1). It can be shown [21] that in this case the exchange interaction between the lowest states of fullerene sites is of conventional Heisenberg form for spins $S = 1/2$, with exchange parameters J^{ij} obtained by averaging their values at fixed JT distortions, $J^{ij}(\alpha_i, \beta_i, \gamma_i, \alpha_j, \beta_j, \gamma_j)$, over the Euler angles parametrising the angular part of nuclear JT distortions of the two fullerene sites (JT coordinates in the troughs). In the case of Anderson's superexchange, which is likely to dominate in fullerenes [34], the dependence of J^{ij} on the angular coordinates of the troughs enters via the electron transfer parameters between adiabatic orbitals of two fullerene sites [36]. Averaging these expressions we obtain the exchange parameters for nearest neighbor (AB) and next-nearest neighbor (AA) C_{60}^{3-} sites corresponding to the main exchange mechanism in Fig. 1 (see the Supplemental Material):

$$J_1^{\text{AB}} = \frac{4}{3U_{\text{AB}}}[(t_{xx}^{\text{AB}})^2 + (t_{yx}^{\text{AB}})^2 + (t_{zx}^{\text{AB}})^2],$$

$$J_1^{\text{AA}} = \frac{4}{9}U_{\text{AA}}[(t_{xx}^{\text{AA}})^2 + (t_{yy}^{\text{AA}})^2 + (t_{zz}^{\text{AA}})^2], \quad (8)$$

where A and B denote two fullerene sublattices merohedrally rotated with respect to each other in A15 Cs_3C_{60} [2, 3]; $t_{\alpha\beta}$ are electron transfer parameters between orbitals of type α and β of two fullerene sites, defined with

respect to corresponding tetragonal axes of the crystal; $U = U_{\parallel} - (10/3)J_{\text{H}} + (4/3)E_{\text{JT}} + V_{\text{eh}}$ is the averaged electron promotion energy between two C_{60}^{3-} . Next in importance is the exchange interaction coming from virtual electron transfers involving empty and doubly occupied adiabatic orbitals ($\psi_2 \rightarrow \psi_3$, $\psi_1 \rightarrow \psi_2$, $\psi_1 \rightarrow \psi_3$ within adiabatic ground state configurations in Fig. 1), which after averaging over JT angular coordinates in the troughs give the following contributions (see the Supplemental Material):

$$J_2^{\text{AB}} = J_1^{\text{AB}} \frac{4E_{\text{JT}} - 16J_{\text{H}}}{3U_{\text{AB}}},$$

$$J_2^{\text{AA}} = J_1^{\text{AA}} \frac{4E_{\text{JT}} - 16J_{\text{H}}}{3U_{\text{AA}}}, \quad (9)$$

that are ferromagnetic ($J_2 < 0$) contrary to contributions (8). The transfer parameters have been evaluated by DFT as matrix elements of Kohn-Sham Hamiltonian between Wannier orbitals constructing from t_{1u} band orbitals [25] (second row in Table III). An independent fit of the dispersion of t_{1u} band [21] (Fig. S1 in Supplemental Material [26]) gives an alternative set of transfer parameters (first row in Table III). The electron repulsion within the same t_{1u} orbitals of C_{60} has been calculated by DFT taking into account the RPA screening in insulating Cs_3C_{60} , $U_{\parallel} = 1.14$ eV, the same for averaged electron-hole attraction for nearest neighbor fullerene sites, $V_{\text{eh}}^{\text{AB}} = -0.34$ eV [25]. For next-nearest neighbour fullerenes we took the value $V_{\text{eh}}^{\text{AA}} = V_{\text{eh}}^{\text{AB}} R_{\text{AB}}/R_{\text{AA}} = -0.29$ eV, where R_{AB} and R_{AA} are the corresponding interfullerene distances. With these values we obtain $U^{\text{AB}} = 0.72$ eV and $U^{\text{AA}} = 0.77$ eV. Then with Eqs. (8) and (9) we obtain for $J_{\text{ex}}^{\text{AB}} = J_1^{\text{AB}} + J_2^{\text{AB}}$ and $J_{\text{ex}}^{\text{AA}} = J_1^{\text{AA}} + J_2^{\text{AA}}$ the values given in Table III. Having in mind that each fullerene has eight nearest and six next-nearest neighbors, we calculate the Néel temperature, $T_{\text{N}} = S(S+1)(8J_{\text{ex}}^{\text{AB}} - 6J_{\text{ex}}^{\text{AA}})/3k$, and find close agreement with experiment for both sets of transfer parameters (Table III). Similar calculations of Weiss temperature, $\Theta = -S(S+1)(8J_{\text{ex}}^{\text{AB}} + 6J_{\text{ex}}^{\text{AA}})/3k$, give, however, lower absolute values than the experimental one, -68 K (Table III).

This can be understood by the closeness of metal-insulator transition in Cs_3C_{60} at ambient pressure, which enhances charge transfer fluctuations between fullerene sites, thus increasing $J_{\text{ex}}^{\text{AB}}$, $J_{\text{ex}}^{\text{AA}}$, and $|\Theta|$. The same reason explains why μ_{eff} [3] extracted from spin susceptibility measurements (1.32) is smaller than the value cor-

responding to $S = 1/2$ (1.73). On the other hand the increase of T_N by these fluctuations will be compensated by its decrease due to quantum spin fluctuations in the antiferromagnetic phase, thus approaching the mean-field T_N calculated above to the experimental value.

These calculations give additional evidence for independent rotational dynamics on fullerene sites in insulating Cs_3C_{60} , since the isotropic Heisenberg model is a fingerprint for such vibronic phase. On the contrary, when the vibronic dynamics is quenched, like in low-symmetry insulating $(\text{NH}_3)\text{K}_3\text{C}_{60}$ [37], the half filled orbitals (ψ_2 in Fig. 1) will be orthogonal for some nearest neighbour fullerenes leading to ferromagnetic exchange interaction similar to J_2^{AB} in Eq. (9). Accordingly, the antiferromagnetic interaction with other fullerene neighbors becomes non-frustrated, resulting in elevated Néel temperature for this fcc lattice, $T_N = 28$ K [37]. For comparison, T_N is only 2.2 K in the cubic fcc fulleride Cs_3C_{60} [4], which is explained by isotropic Heisenberg exchange interaction arising in this fulleride due to unquenched dynamical JTE on C_{60}^{3-} sites and, therefore, unavoidable frustration of antiferromagnetic exchange interactions in this lattice.

N. I. would like to acknowledge the financial support from Flemish Science Foundation (FWO) and the GOA grant from KU Leuven.

-
- [1] O. Gunnarsson, *Revs. Mod. Phys.* **69**, 575 (1997).
 - [2] A. Y. Ganin, Y. Takabayashi, Y. Z. Khimyak, S. Margadonna, A. Tamai, M. J. Rosseinsky, and K. Prassides, *Nat. Mater.* **7**, 367 (2008).
 - [3] Y. Takabayashi, A. Y. Ganin, P. Jeglič, D. Arčon, T. Takano, Y. Iwasa, Y. Ohishi, M. Takata, N. Takeshita, K. Prassides, and M. J. Rosseinsky, *Science* **323**, 158 (2009).
 - [4] A. Y. Ganin, Y. Takabayashi, P. Jeglič, D. Arčon, A. Potočnik, P. J. Baker, Y. Ohishi, M. T. McDonald, M. D. Tzirakis, A. McLennan, G. R. Darling, M. Takata, M. J. Rosseinsky, and K. Prassides, *Nature* **466**, 221 (2010).
 - [5] P. Jeglič, D. Arčon, A. Potočnik, A. Y. Ganin, Y. Takabayashi, M. J. Rosseinsky, and K. Prassides, *Phys. Rev. B* **80**, 195424 (2009).
 - [6] Y. Ihara, H. Alloul, P. Wzietek, D. Pontiroli, M. Mazzani, and M. Riccò, *Phys. Rev. Lett.* **104**, 256402 (2010).
 - [7] S. Kawasaki, J. Fukui, T. Motoyama, Y. Suzuki, S. Shibusaki, and G. q. Zheng, *J. Phys. Soc. Jpn.* **82**, 014709 (2013).
 - [8] M. Capone, M. Fabrizio, C. Castellani, and E. Tosatti, *Science* **296**, 2364 (2002).
 - [9] J. E. Han, O. Gunnarsson, and V. H. Crespi, *Phys. Rev. Lett.* **90**, 167006 (2003).
 - [10] M. Capone, M. Fabrizio, C. Castellani, and E. Tosatti, *Revs. Mod. Phys.* **81**, 943 (2009).
 - [11] Y. Maniwa, T. Saito, A. Ohi, K. Mizoguchi, K. Kumi, K. Kukughi, I. Ikemoto, S. Suzuki, Y. Achiba, M. Kosaka, K. Tanigaki, and T. Ebbesen, *J. Phys. Soc. Jpn.* **63**, 1139 (1994).
 - [12] O. Gunnarsson, H. Handschuh, P. S. Bechthold, B. Kessler, G. Ganteför, and W. Eberhardt, *Phys. Rev. Lett.* **74**, 1875 (1995).
 - [13] N. Iwahara, T. Sato, K. Tanaka, and L. F. Chibotaru, *Phys. Rev. B* **82**, 245409 (2010).
 - [14] P. Durand, G. R. Darling, Y. Dubitsky, A. Zaopo, and M. J. Rosseinsky, *Nat. Mater.* **2**, 605 (2003).
 - [15] L. F. Chibotaru, *Phys. Rev. Lett.* **94**, 186405 (2005).
 - [16] G. Klupp, P. Matus, K. Kamarás, A. Y. Ganin, A. McLennan, M. J. Rosseinsky, Y. Takabayashi, M. T. McDonald, and K. Prassides, *Nat. Commun.* **3**, 912 (2012).
 - [17] M. C. M. O'Brien, *Phys. Rev. B* **53**, 3775 (1996).
 - [18] A. Auerbach, N. Manini, and E. Tosatti, *Phys. Rev. B* **49**, 12998 (1994).
 - [19] I. B. Bersuker and V. Z. Polinger, *Vibronic Interactions in Molecules and Crystals* (Springer-Verlag, Berlin and Heidelberg, 1989).
 - [20] We use sets (6) and (3) of Table I and II in Ref. [13] for sets (2) and (3), respectively.
 - [21] N. Iwahara and L. F. Chibotaru, (to be published).
 - [22] R. L. Martin and J. P. Ritchie, *Phys. Rev. B* **48**, 4845 (1993).
 - [23] C. C. Chancey and M. C. M. O'Brien, *The Jahn-Teller Effect in C_{60} and Other Icosahedral Complexes* (Princeton University Press, Princeton, 1997).
 - [24] A. Potočnik, N. Manini, M. Komelj, E. Tosatti, and D. Arčon, *Phys. Rev. B* **86**, 085109 (2012).
 - [25] Y. Nomura, K. Nakamura, and R. Arita, *Phys. Rev. B* **85**, 155452 (2012).
 - [26] See Supplemental Material for vibronic couplings, frequencies of Cs_3C_{60} , energy band fitted to the model Hamiltonian, and derivation of Eqs. (8) and (9).
 - [27] J. L. Dunn and C. A. Bates, *Phys. Rev. B* **52**, 5996 (1995).
 - [28] L. M. Sindi, I. D. Hands, J. L. Dunn, and C. Bates, *J. Mol. Struct.* **838**, 78 (2007).
 - [29] A. J. Lakin, I. D. Hands, C. Bates, and J. L. Dunn, in *Vibronic Interactions and the Jahn-Teller Effect: Theory and Applications*, edited by M. Atanasov, C. Daul, and P. L. W. Tregenna-Piggott (Springer-Verlag, Berlin, 2012), p. 231.
 - [30] N. Koga and K. Morokuma, *Chem. Phys. Lett.* **196**, 191 (1992).
 - [31] H. Ramanantoanina, M. Gruden-Pavlovic, M. Zlatar, and C. Daul, *Int. J. Quant. Chem.* **113**, 802 (2012).
 - [32] A larger second order JT effect has been predicted in Ref. [33], where potential energy wells of ca 120 cm^{-1} have been predicted at D_{5d} symmetry points of the lowest APES. Note, however, that even this energy is much smaller than the energy gain due to delocalization of JT deformations in the trough of the lowest APES (ca 700 cm^{-1} according to Table II).
 - [33] M. Saito, *Phys. Rev. B* **65**, 220508(R) (2002).
 - [34] The contribution of direct (potential) exchange is expected to be small because of small overlap density of magnetic orbitals. The latter can only be important when the magnetic orbitals at two sites have significant hybridization with some bridging atoms [35]. This is not the case in the ionic lattice of Cs_3C_{60} where the Mulliken charge of Cs is very close to +1 (0.995) as obtained from our DFT calculations.
 - [35] O. Kahn, *Molecular Magnetism* (VCH, New York, 1993), pp.179-180.
 - [36] L. F. Chibotaru, *J. Mol. Struct.* **838**, 53 (2007).
 - [37] S. Margadonna, K. Prassides, H. Shimoda, T. Takenobu, and Y. Iwasa, *Phys. Rev. B* **64**, 132414 (2001).

Supplemental Material
for
“Dynamical Jahn–Teller effect and antiferromagnetism in Cs₃C₆₀”

TABLE S1. Dimensionless vibronic coupling constants g_μ and JT stabilization energies from individual modes $E_{JT,\mu}$ (meV) for C₆₀[−]. Set (1) is obtained from fragment DFT calculations of Cs₃C₆₀ and sets (2) and (3) are derived from DFT calculations and PES of C₆₀[−], respectively [S1].

μ	Set (1)		Set (2)		Set (3)	
	g_μ	$E_{JT,\mu}$	g_μ	$E_{JT,\mu}$	g_μ	$E_{JT,\mu}$
1	0.413	2.9	0.436	3.2	0.490	4.1
2	0.484	6.3	0.498	6.7	0.515	7.2
3	0.437	8.4	0.418	7.7	0.455	9.1
4	0.258	3.2	0.259	3.2	0.300	4.3
5	0.210	3.0	0.211	3.0	0.280	5.3
6	0.137	1.5	0.126	1.2	0.235	4.3
7	0.383	13.0	0.398	14.0	0.435	16.8
8	0.332	10.8	0.338	11.2	0.260	6.6
E_{JT}		49.1		50.2		57.7

TABLE S2. Frequencies of h_g vibrational modes (cm^{−1}) of isolated C₆₀ and in A15 Cs₃C₆₀ derived from DFT calculations.

C ₆₀	A15 Cs ₃ C ₆₀	
h_g	t_g	e_g
264.8	271.4	271.7
435.0	427.1	431.7
721.1	696.6	699.4
784.5	786.2	786.1
1123.0	1117.5	1117.9
1265.2	1249.0	1250.1
1442.1	1448.0	1449.2
1608.3	1598.2	1599.7

Frequencies of C₆₀ and A15 Cs₃C₆₀ are shown in Table S2. For the estimation of the splitting of h_g vibrational modes by the cubic environment of each fullerene in Cs₃C₆₀, the frequencies of the e_g and the t_g modes are used. The frequencies of an isolated neutral C₆₀ are given (i) to prove that our calculations of frequencies are reliable and (ii) to see how much the charging effect changes the frequencies. The obtained frequencies of C₆₀ are close to the experimental ones [S2] and to DFT values obtained by other authors [S2, S3].

Derivation of Eqs. (8) and (9)[S4]

Suppose the Jahn–Teller deformation of each fullerene

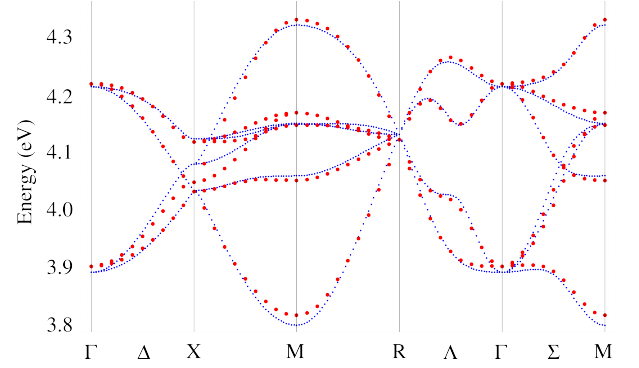


FIG. S1. (color online) Band structure of A15 Cs₃C₆₀ obtained by DFT calculation (red circles) and the effective model with parameters in Table IV (blue dots).

is fixed at first. The Hamiltonian for two sites (i, j) is

$$\hat{H} = \hat{H}_t + \hat{H}_{JT} + \hat{H}_{bi} + \hat{H}_{eh}, \quad (S1)$$

$$\hat{H}_t = \sum_{\lambda\lambda'} \sum_{\sigma} t_{\lambda\lambda'} \left(\hat{c}_{i\lambda\sigma}^\dagger \hat{c}_{j\lambda'\sigma} + \hat{c}_{j\lambda'\sigma}^\dagger \hat{c}_{i\lambda\sigma} \right), \quad (S2)$$

$$\hat{H}_{JT} = \sum_{m=i,j} 3E_{JT} \sum_{\sigma} (\hat{n}_{m3\sigma} - \hat{n}_{m1\sigma}) + 3E_{JT}, \quad (S3)$$

$$\begin{aligned} \hat{H}_{bi} = & \sum_{m=i,j} \frac{1}{2} \sum_{\lambda=1}^3 \sum_{\sigma} [U_{\parallel} \hat{n}_{m\lambda\sigma} \hat{n}_{m\lambda,-\sigma} \\ & + U_{\perp} \sum_{\lambda'(\neq\lambda)} \sum_{\sigma'} \hat{n}_{m\lambda\sigma} \hat{n}_{m\lambda'\sigma'} - J_H \sum_{\lambda'(\neq\lambda)} (\hat{n}_{m\lambda\sigma} \hat{n}_{m\lambda'\sigma} \\ & - \hat{c}_{m\lambda\sigma}^\dagger \hat{c}_{m\lambda'\sigma} \hat{c}_{m\lambda,-\sigma}^\dagger \hat{c}_{m\lambda',-\sigma} \\ & - \hat{c}_{m\lambda\sigma}^\dagger \hat{c}_{m\lambda'\sigma} \hat{c}_{m\lambda',-\sigma}^\dagger \hat{c}_{m\lambda,-\sigma})], \end{aligned} \quad (S4)$$

$$\hat{H}_{eh} = -V_{eh} \sum_{\lambda\sigma} \hat{n}_{i\lambda\sigma} \sum_{\lambda'\sigma'} \hat{n}_{j\lambda'\sigma'}, \quad (S5)$$

where $m(=i, j)$ is the index for site, $\lambda, \lambda' (= 1, 2, 3)$ the indices for adiabatic orbital (see Fig. 1 in the text), $\sigma(=\uparrow, \downarrow)$ the spin projection, $\hat{c}_{m\lambda\sigma}^\dagger$ and $\hat{c}_{m\lambda\sigma}$ the creation and annihilation operators, respectively, $\hat{n}_{m\lambda\sigma}$ the number operator, E_{JT} the Jahn–Teller stabilization energy for C₆₀[−], $t_{\lambda\lambda'}$ the transfer parameter, U_{\parallel} the intraorbital onsite Coulomb repulsion, $U_{\perp}(=U_{\parallel} - 2J_H)$ the interorbital onsite Coulomb repulsion, J_H is the Hund’s coupling, and $V_{eh}(< 0)$ is the intersite electron-hole attraction.

We regard $\hat{H}_{bi} + \hat{H}_{JT} + \hat{H}_{eh}$ as unperturbed Hamiltonian and \hat{H}_t as perturbation. The unperturbed Hamiltonian is divided into two terms: first term \hat{H}_0 depends

only on the sum of number operators, the other \hat{H}' consists of remaining terms.

$$\hat{H}_0 = \sum_{m=i,j} \left[\frac{U}{2} \sum_{\lambda\sigma} \left(\hat{n}_{m\lambda\sigma} \hat{n}_{m\lambda,-\sigma} + \sum_{\lambda'(\neq\lambda)} \sum_{\sigma'} \hat{n}_{m\lambda\sigma} \hat{n}_{m\lambda'\sigma'} \right) + E_{\text{JT}} \right] + \hat{H}_{\text{eh}}, \quad (\text{S6})$$

$$\begin{aligned} \hat{H}' = \sum_{m=i,j} \left\{ E_{\text{JT}} \sum_{\sigma} (\hat{n}_{m3\sigma} - \hat{n}_{m1\sigma}) + \frac{A}{2} \sum_{\lambda\sigma} \hat{n}_{m\lambda\sigma} \hat{n}_{m\lambda,-\sigma} - \frac{1}{2} \sum_{\lambda\sigma} \left[B \sum_{\lambda'(\neq\lambda)} \sum_{\sigma'} \hat{n}_{m\lambda\sigma} \hat{n}_{m\lambda'\sigma'} \right. \right. \\ \left. \left. + J_{\text{H}} \sum_{\lambda'(\neq\lambda)} \left(\hat{n}_{m\lambda\sigma} \hat{n}_{m\lambda'\sigma} - \hat{c}_{m\lambda\sigma}^\dagger \hat{c}_{m\lambda'\sigma} \hat{c}_{m\lambda,-\sigma}^\dagger \hat{c}_{m\lambda',-\sigma} - \hat{c}_{m\lambda\sigma}^\dagger \hat{c}_{m\lambda'\sigma} \hat{c}_{m\lambda',-\sigma}^\dagger \hat{c}_{m\lambda,-\sigma} \right) \right] \right\}, \quad (\text{S7}) \end{aligned}$$

where U is an promotion energy

$$U = U_{\parallel} - \frac{10}{3} J_{\text{H}} + \frac{4}{3} E_{\text{JT}} + V_{\text{eh}}, \quad (\text{S8})$$

A is

$$A = \frac{10}{3} J_{\text{H}} - \frac{4}{3} E_{\text{JT}}, \quad (\text{S9})$$

and B is

$$B = -\frac{4}{3} J_{\text{H}} + \frac{4}{3} E_{\text{JT}}. \quad (\text{S10})$$

Performing a unitary transformation, we remove \hat{H}_t in the first order.

$$\hat{H}_{\text{eff}} = \hat{H}_0 + \hat{H}' + \frac{1}{U} \hat{H}_t \hat{H}_t - \frac{1}{2U^2} \left[[\hat{H}', \hat{H}_t], \hat{H}_t \right]. \quad (\text{S11})$$

Since spin-orbit coupling is not included, orbital and spin degrees of freedom can be separated. The interaction between site i and site j is

$$\hat{H}^{ij} = \hat{K}^{ij} + \hat{J}^{ij} \left(\mathbf{S}_i \cdot \mathbf{S}_j + \frac{1}{2} \right). \quad (\text{S12})$$

Here, \hat{K}^{ij} and \hat{J}^{ij} are operators which act on orbital space, and \mathbf{S} is the spin operator.

To obtain the superexchange Hamiltonian, \hat{H}_{eff} is averaged by the ground vibronic states of the fullerenes. First, \hat{H}_{eff} is averaged by electronic part of the vibronic state:

$$\hat{H}_{\text{ex}} = K^{ij} + \left(J_1^{ij} + J_2^{ij} \right) \left(\mathbf{S}_i \cdot \mathbf{S}_j + \frac{1}{2} \right), \quad (\text{S13})$$

where K^{ij} is

$$\begin{aligned} K^{ij} = & -2 \frac{\left(t_{13}^{ij} \right)^2 + \left(t_{31}^{ij} \right)^2}{U} \left(1 - \frac{2E_{\text{JT}} + J_{\text{H}}}{3U} \right) \\ & - \frac{\left(t_{12}^{ij} \right)^2 + \left(t_{21}^{ij} \right)^2}{U} \left(1 - \frac{E_{\text{JT}} - J_{\text{H}}}{3U} \right) \\ & - \frac{\left(t_{23}^{ij} \right)^2 + \left(t_{32}^{ij} \right)^2}{U} \left(1 + \frac{E_{\text{JT}} - 7J_{\text{H}}}{3U} \right) \\ & - 2 \frac{\left(t_{22}^{ij} \right)^2}{U} \left(1 + \frac{4E_{\text{JT}} - 10J_{\text{H}}}{3U} \right), \quad (\text{S14}) \end{aligned}$$

J_1^{ij} and J_2^{ij} are

$$\begin{aligned} J_1^{ij} = & 4 \frac{\left(t_{22}^{ij} \right)^2}{U}, \quad (\text{S15}) \\ J_2^{ij} = & 4 \frac{\left(t_{22}^{ij} \right)^2}{U} \frac{4E_{\text{JT}} - 10J_{\text{H}}}{3U} \\ & - 2 \frac{\left(t_{12}^{ij} \right)^2 + \left(t_{21}^{ij} \right)^2 + \left(t_{23}^{ij} \right)^2 + \left(t_{32}^{ij} \right)^2}{U} \frac{J_{\text{H}}}{U}, \quad (\text{S16}) \end{aligned}$$

respectively. K^{ij} and J^{ij} depend on the Euler angles (α, β, γ) parametrizing the angular part of the Jahn–Teller deformation.

To complete the averaging of \hat{H}_{eff} by the ground vibronic states, J^{ij} 's are averaged over the Euler angles. The transfer parameters $t_{\lambda\lambda'}$ between nearest neighbour sites (AB) and next nearest neighbours (AA) are described by $t_{\alpha\beta}$ ($\alpha, \beta = x, y, z$) as follows:

$$\begin{pmatrix} t_{11}^{\text{AB}} & t_{12}^{\text{AB}} & t_{13}^{\text{AB}} \\ t_{21}^{\text{AB}} & t_{22}^{\text{AB}} & t_{23}^{\text{AB}} \\ t_{31}^{\text{AB}} & t_{32}^{\text{AB}} & t_{33}^{\text{AB}} \end{pmatrix} = B_P(\alpha_i) C_P(\beta_i) D_P(\gamma_i) \begin{pmatrix} t_{xx}^{\text{AB}} & t_{zx}^{\text{AB}} & t_{yx}^{\text{AB}} \\ t_{yx}^{\text{AB}} & t_{xx}^{\text{AB}} & t_{zx}^{\text{AB}} \\ t_{zx}^{\text{AB}} & t_{yx}^{\text{AB}} & t_{xx}^{\text{AB}} \end{pmatrix} D_P^\dagger(\gamma_j) C_P^\dagger(\beta_j) B_P^\dagger(\alpha_j), \quad (\text{S17})$$

$$\begin{pmatrix} t_{11}^{\text{AA}} & t_{12}^{\text{AA}} & t_{13}^{\text{AA}} \\ t_{21}^{\text{AA}} & t_{22}^{\text{AA}} & t_{23}^{\text{AA}} \\ t_{31}^{\text{AA}} & t_{32}^{\text{AA}} & t_{33}^{\text{AA}} \end{pmatrix} = B_P(\alpha_i) C_P(\beta_i) D_P(\gamma_i) \begin{pmatrix} t_{xx}^{\text{AA}} & 0 & 0 \\ 0 & t_{yy}^{\text{AA}} & 0 \\ 0 & 0 & t_{zz}^{\text{AA}} \end{pmatrix} D_P^\dagger(\gamma_j) C_P^\dagger(\beta_j) B_P^\dagger(\alpha_j), \quad (\text{S18})$$

where

$$B_P(\alpha) = \begin{pmatrix} \cos \alpha & \sin \alpha & 0 \\ -\sin \alpha & \cos \alpha & 0 \\ 0 & 0 & 1 \end{pmatrix}, \quad (\text{S19})$$

$$C_P(\beta) = \begin{pmatrix} \cos \beta & 0 & -\sin \beta \\ 0 & 1 & 0 \\ \sin \beta & 0 & \cos \beta \end{pmatrix}, \quad (\text{S20})$$

$$D_P(\gamma) = \begin{pmatrix} \cos \gamma & \sin \gamma & 0 \\ -\sin \gamma & \cos \gamma & 0 \\ 0 & 0 & 1 \end{pmatrix}. \quad (\text{S21})$$

The averages of the squared transfer parameters $t_{\lambda\lambda'}^2$ are given by

$$\begin{aligned} \langle (t_{\lambda\lambda'}^{\text{AB}})^2 \rangle &= \frac{1}{4\pi^4} \int_0^\pi d\alpha_i \int_0^{\pi/2} d\beta_i \sin \beta_i \int_0^{2\pi} d\gamma_i \\ &\times \int_0^\pi d\alpha_j \int_0^{\pi/2} d\beta_j \sin \beta_j \int_0^{2\pi} d\gamma_j (t_{\lambda\lambda'}^{\text{AB}})^2 \end{aligned} \quad (\text{S22})$$

$$= \frac{(t_{xx}^{\text{AB}})^2 + (t_{yx}^{\text{AB}})^2 + (t_{zx}^{\text{AB}})^2}{3}, \quad (\text{S23})$$

$$\begin{aligned} \langle (t_{\lambda\lambda'}^{\text{AA}})^2 \rangle &= \frac{1}{4\pi^4} \int_0^\pi d\alpha_i \int_0^{\pi/2} d\beta_i \sin \beta_i \int_0^{2\pi} d\gamma_i \\ &\times \int_0^\pi d\alpha_j \int_0^{\pi/2} d\beta_j \sin \beta_j \int_0^{2\pi} d\gamma_j (t_{\lambda\lambda'}^{\text{AA}})^2 \end{aligned} \quad (\text{S24})$$

$$= \frac{(t_{xx}^{\text{AA}})^2 + (t_{yy}^{\text{AA}})^2 + (t_{zz}^{\text{AA}})^2}{9}. \quad (\text{S25})$$

With use of Eq. (S23), the superexchange amplitude for the nearest neighbour is

$$J_{\text{ex}}^{\text{AB}} = J_1^{\text{AB}} + J_2^{\text{AB}}, \quad (\text{S26})$$

$$J_1^{\text{AB}} = \frac{4}{3U_{\text{AB}}} \left[(t_{xx}^{\text{AB}})^2 + (t_{yx}^{\text{AB}})^2 + (t_{zx}^{\text{AB}})^2 \right], \quad (\text{S27})$$

$$J_2^{\text{AB}} = J_1^{\text{AB}} \frac{4E_{\text{JT}} - 16J_{\text{H}}}{3U_{\text{AB}}}. \quad (\text{S28})$$

Similarly, using Eq. (S25), the superexchange amplitude for the next nearest neighbour is

$$J_{\text{ex}}^{\text{AA}} = J_1^{\text{AA}} + J_2^{\text{AA}}, \quad (\text{S29})$$

$$J_1^{\text{AA}} = \frac{4}{9U_{\text{AA}}} \left[(t_{xx}^{\text{AA}})^2 + (t_{yy}^{\text{AA}})^2 + (t_{zz}^{\text{AA}})^2 \right], \quad (\text{S30})$$

$$J_2^{\text{AA}} = J_1^{\text{AA}} \frac{4E_{\text{JT}} - 16J_{\text{H}}}{3U_{\text{AA}}}. \quad (\text{S31})$$

Eqs. (S27) and (S30) are Eqs. (8), and Eqs. (S28) and (S31) are Eqs. (9) in the text.

[S1] N. Iwahara, T. Sato, K. Tanaka, and L. F. Chibotaru, Phys. Rev. B **82**, 245409 (2010).

[S2] O. Gunnarsson, Revs. Mod. Phys. **69**, 575 (1997).

[S3] C. H. Choi, M. Kertesz, and L. Mihaly, J. Phys. Chem. A **104**, 102 (2000)

[S4] L. F. Chibotaru, J. Mol. Struct. **838**, 53 (2007).